Journal of Applied Physics

Peak states of molybdenum single crystals shock compressed to high stresses

Cite as: J. Appl. Phys. **129**, 245906 (2021); https://doi.org/10.1063/5.0054395
Submitted: 17 April 2021 . Accepted: 09 June 2021 . Published Online: 30 June 2021

Tomoyuki Oniyama, Yogendra M. Gupta, and Guruswami Ravichandran

Journal of Applied Physics ARTICLE scitation.org/journal/jap

Peak states of molybdenum single crystals shock compressed to high stresses

Cite as: J. Appl. Phys. **129**, 245906 (2021); doi: 10.1063/5.0054395
Submitted: 17 April 2021 · Accepted: 9 June 2021 ·
Published Online: 30 June 2021

View Online Export Citation CrossMark

Tomoyuki Oniyama,[1,a)] Yogendra M. Gupta,[2] and Guruswami Ravichandran[1]

AFFILIATIONS

[1]Division of Engineering and Applied Science, California Institute of Technology, Pasadena, California 91125, USA
[2]Institute for Shock Physics and Department of Physics and Astronomy, Washington State University, Pullman, Washington 99164, USA

[a)]**Author to whom correspondence should be addressed:** toniyama@alumni.caltech.edu

ABSTRACT

To determine crystal anisotropy effects at high stresses, peak states behind the plastic shock waves were examined in BCC single crystals. Using plate impact experiments, molybdenum (Mo) single crystals were shock compressed up to 190 GPa elastic impact stress along [100], [110], and [111] orientations. Laser interferometry was used to measure wave velocities and particle velocity profiles at the Mo–LiF window interface. These data were analyzed to obtain in-material quantities in the peak states. The Hugoniots for [100] and [110] orientations were comparable, but the Hugoniot for the [111] orientation was different from the other two orientations. Also, these Mo single crystal Hugoniots display differences from the polycrystalline Mo Hugoniots. Although none of the differences can be considered large, the present results demonstrate that, unlike FCC metal single crystals (Cu, Al), some anisotropy is preserved in Mo single crystal Hugoniots even at high stresses.

I. INTRODUCTION

Shock wave experiments on metal single crystals are important for gaining insight into elastic-plastic deformation mechanisms at high stresses and on short time scales (ns to μs) and for characterizing the peak states at stresses not achievable by other methods. The combination of well-characterized plate impact experiments—resulting in uniaxial strain loading—and single crystals can be used to examine the role of crystal anisotropy on shock wave-induced plastic deformation by exploring the role of different slip/twinning mechanisms. Additionally, single crystal experiments avoid complications arising from wave interactions at grain boundaries.

Due to the features noted above, shock wave experiments have been carried out on a wide range of metal and ionic single crystals.[1–15] However, most of the past experimental studies were carried out at low peak stresses ranging from a few to ∼20 GPa. In contrast, elastic-plastic deformation of single crystals shock compressed to high stresses (above 50 GPa) has been studied minimally. To address this need, we previously reported on the role of crystal anisotropy on elastic-plastic deformation in molybdenum (Mo) single crystals shocked to 110 GPa along different crystal orientations.[16] The focus of our earlier work was on understanding the dependence of the elastic wave amplitude on peak stress (20 to 110 GPa) and on gaining insight into the slip systems activated for shock compression along different crystal orientations.

Apart from elastic wave amplitudes, peak states have been examined minimally in shock compressed metal single crystals at high stresses (above 50 GPa). Almost all of the studies to date regarding peak states or the Hugoniot relations in metals at high stresses have focused on polycrystalline materials.[17] In this work, we report on experimental measurements of peak states or Hugoniots in Mo single crystals shocked up to 190 GPa along three crystal orientations. To the best of our knowledge, peak states have not been measured at high stresses in BCC metal single crystals. However, two studies on shock wave experiments at high stresses have been reported on FCC metal single crystals.[18,19]

Chau *et al.*[18] examined the response of copper (Cu) single crystals up to 67 GPa and reported that the Hugoniots along three different orientations were very similar and agreed well with the polycrystalline Cu Hugoniot.[20] Choudhuri and Gupta[19] examined the response of aluminum (Al) single crystals to 70 GPa and reported that, within experimental uncertainties, the Hugoniots for three different orientations were indistinguishable. However, the Al

work showed distinct anisotropy in longitudinal sound speeds and moduli in the peak states.

For both Cu and Al single crystals, the elastic wave amplitudes or the Hugoniot elastic limits (HEL) are very small and range between ~0.1 and 0.3 GPa. In contrast, the elastic wave amplitudes for Mo single crystals are larger than Cu and Al by more than an order of magnitude and range between ~4 and ~9 GPa depending on the crystal orientation and peak stresses. This large difference between the elastic wave amplitudes raises a number of questions indicated below that are addressed in this work.

Does the anisotropy observed at the elastic limit also manifest at the peak states in Mo single crystals shock compressed to high stresses? Will the peak states for these orientations in Mo single crystals show differences or will they be similar to the nearly identical response observed in Cu and Al? How will the Hugoniots for the three orientations compare with the Hugoniot measured for polycrystalline Mo? Using wave profile measurements in Mo single crystals subjected to high velocity planar impacts and by analyzing these data, we provide answers to these questions.

The experimental details are briefly summarized in Sec. II, and the results are presented in Sec. III. The calculations of in-material quantities at the peak state are summarized in Sec. IV; this section also compares the Hugoniot relations for the three orientations and with polycrystalline Mo.[17] The main findings of this work are summarized in Sec. V.

II. EXPERIMENTAL METHOD

The experimental configuration shown in Fig. 1 and the experimental procedures used for this work were the same as described in Ref. 16. Hence, only a brief summary is presented here. The Mo single crystals were obtained from Accumet Materials Co. and 2 mm thick samples were cut from the single crystal bars. The sample thickness was kept constant for all of the experiments in this study. The density and sound speed were measured to characterize the samples at ambient condition, and the results are shown in Table I. The sample orientations were within 1.5° as noted in Ref. 16. In each experiment, the particle velocity at the Mo sample–LiF window interface was measured using laser interferometry (Velocity Interferometer System for any Reflector, VISAR[21–23]).

Table II summarizes the experimental parameters. Elastic impact stress (EIS) in Table II provides a measure of the stress amplitude imparted to single crystals along different orientations. Despite crystal anisotropy, the EIS enables a consistent comparison of the results for different crystal orientations. The EIS was calculated from the continuity of longitudinal stress and particle velocity at the buffer–Mo sample interface. In the EIS calculation, the elastic Hugoniot relation for Mo single crystals[13,14] based on finite elasticity[6] and known Hugoniot relations for the impactor and the buffer[24,25] were used. The experiments along [100], [111], and [110] orientations are referred to as A1–A7, B1–B6, and C1–C5, respectively. Experiments (A2,A3), (A5,A6), and (B1,B2) are pairs of experiments under nearly identical conditions. We note that experimental parameters for experiments A1–A6, B1–B5, and C1–C3 listed in Table II were presented in Ref. 16. However, as noted above, the focus of our earlier work was entirely on elastic wave amplitudes and not on peak states.

In order to achieve an accurate measurement of the time of arrival at the front surface of the Mo sample, the impactor tilt was taken into account in the following manner. In each experiment, the arrival times at three outer probes were measured. That gives the distance to the impactor from the buffer surface measured at three probe locations upon impact at one of the probe locations. Since the deformation of the impactor is axisymmetric due to its loading and is taken into account as described below, we can determine the time of impact at the center of the Mo sample.

Experiments A1–A3, B1–B2, and C1–C2 were conducted on a powder gun, and the remainder of the experiments were conducted on a two-stage light gas gun. For experiments whose projectile velocity was close to the upper limit at each facility, we conducted a trial ("test shot") experiment to quantify the bowing of the impactor at each velocity level. In each test shot, a projectile was launched against a target consisted only with LiF window. Al mirror was vapor deposited onto the front surface of the LiF window that got impacted by the impactor. Four VISAR probes were placed at the same locations as experiments, and they were focused on the Al mirror. The moment when the velocity became nonzero was

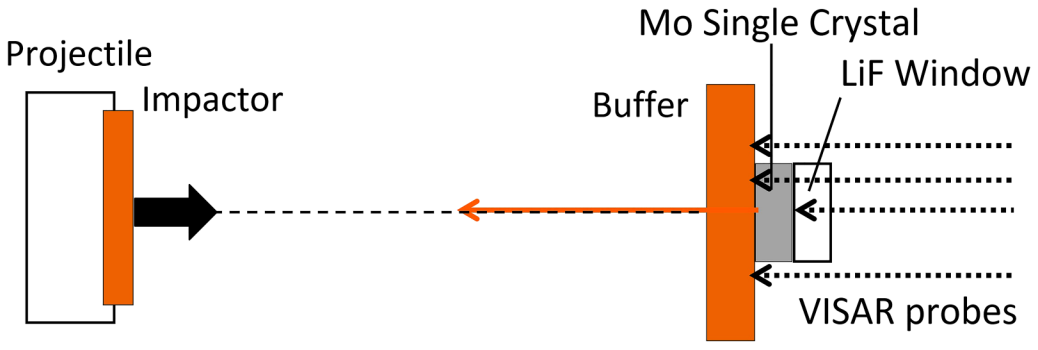

FIG. 1. Schematic of the plate impact experimental configuration. In all experiments, the impactor and the buffer were of the same material to avoid wave reflections from the impactor/buffer interface. Reproduced from Oniyama *et al.*, J. Appl. Phys. **127**, 205902 (2020). Copyright 2000 AIP Publishing LLC.

TABLE I. Ambient properties of Mo single crystals.

Orientation	Density (g/cm^3)	Longitudinal sound speed (km/s)	Shear sound speed (km/s)	Bulk sound speed (km/s)
[100]	10.22 ± 0.06	6.746 ± 0.008	3.261 ± 0.005	5.597 ± 0.011
[111]		6.319 ± 0.005	3.666 ± 0.014	4.692 ± 0.017
[110][a]		6.432 ± 0.003	3.850 ± 0.004	4.648 ± 0.007
			3.264 ± 0.004	5.212 ± 0.005

[a]Acoustic tensor corresponding to wave propagation along the [110] orientation in a cubic crystal has three distinct eigenvalues.

recorded as the arrival time at each location. From the arrival times at three outer probes, we can calculate the arrival time at the center probe, assuming no deformation. The difference of the actual arrival time and the calculated arrival time at the center gives the deformation at the center. Then, we applied the bowing correction to each experiment to account for impactor deformation. The bowing corrections are shown at the bottom of Table III.

III. EXPERIMENTAL RESULTS

The complete wave profiles measured at the Mo–LiF interface at different impact stresses are shown in Figs. 2–4. The times shown in Figs. 2–4 are relative to the arrival of the shock wave at the Mo front surface and are divided by the sample thickness to account for slight differences in sample thicknesses. This approach enables shock velocity comparisons between the experiments. Wave profiles for each orientation are briefly discussed below, and the same are compared in Sec. III D.

A. [100] orientation

Figure 2 shows that in experiments A1–A6, a two wave structure—an elastic wave followed by a plastic shock wave—was observed. Only a single wave was observed in A7. As discussed in Ref. 16, experiments A2 and A5 are excluded from further discussion due to the anomalous behavior observed at the elastic limit. In Fig. 2, one can observe that the particle velocity behind the plastic shock wave and the plastic shock velocity, as expected, increased with increasing impact stress; at the highest impact stress (A7), the plastic shock wave overtakes the elastic shock wave resulting in a single wave.

B. [111] orientation

Figure 3 shows that in experiments B1–B5, a two wave structure was observed. The single wave structure was observed only in B6. Similar to the [100] orientation, the particle velocity behind the plastic shock wave and the plastic shock velocity increased with the increasing impact stress. Experiments B1 and B2 demonstrated good reproducibility of the measured profiles.

TABLE II. Experimental parameters of the plate impact experiments.

Exp. number	Loading direction	Sample thickness (mm)	Impactor/ bufffer material	Impactor thickness (mm)	Buffer thickness (mm)	Window thickness (mm)	Projectile velocity (km/s)	Elastic impact stress (GPa)	Impact tilt (mrad)
A1	[100]	2.019	1050Al	1.831	0.956	6.366	1.549	23.2	0.392
A2		2.010	C101Cu	1.717	0.924	6.363	2.099	65.7	2.61
A3		2.011	C101Cu	1.686	0.921	6.363	2.113	66.2	1.27
A4		2.030	C101Cu	3.058	0.921	6.362	2.680	89.1	3.05
A5		2.027	C101Cu	1.094	0.926	6.346	3.126	108.6	2.32
A6		2.030	C101Cu	1.109	0.923	6.397	3.291	116.1	4.80
A7		2.022	C101Cu	3.086	0.932	6.368	4.637	183.9	1.94
B1	[111]	2.027	1050Al	1.842	0.915	6.366	1.595	23.9	0.55
B2		2.029	1050Al	1.803	0.916	6.342	1.599	24.0	0.30
B3		2.009	C101Cu	1.704	0.928	6.364	2.106	67.4	0.97
B4		2.043	C101Cu	3.052	0.925	6.055	2.710	93.7	4.99
B5		2.027	C101Cu	1.101	0.927	6.344	3.149	114.6	3.18
B6		2.034	C101Cu	3.049	0.931	6.117	4.634	197.5	3.07
C1	[110]	2.021	1050Al	1.778	0.909	6.365	1.571	23.5	0.61
C2		2.018	C101Cu	1.708	0.934	6.360	2.110	67.0	1.28
C3		2.032	C101Cu	3.047	0.944	6.053	2.676	90.9	3.91
C4		2.029	C101Cu	1.097	0.920	6.054	3.151	112.9	4.33
C5		2.040	C101Cu	3.013	0.940	6.117	4.639	193.1	3.30

TABLE III. Calculated in-material quantities at the peak state.

Exp. number	Loading direction	Sample thickness (mm)	Elastic impact stress (GPa)	Plastic[a] shock velocity (km/s)	Measured particle velocity (km/s)	In-material quantities: Particle velocity (km/s)	In-material quantities: Peak stress (GPa)	In-material quantities: Density (g/cm^3)
A1	[100]	2.019	23.2	5.39±0.10	0.588±0.006	0.384±0.024	22.0±1.4	10.979±0.053
A2[b]		2.010	65.7	6.16±0.12[c]	1.40±0.02	0.918±0.036	58.0±2.5	12.001±0.089
A3		2.011	66.2	6.21±0.12[c]	1.41±0.02	0.924±0.036	58.9±2.5	11.996±0.090
A4		2.030	89.1	6.57±0.07	1.80±0.02	1.18±0.03	79.3±2.1	12.449±0.073
A5[b]		2.027	108.6	6.85±0.12[d]	2.10±0.03	1.37±0.04	96.2±3.1	12.783±0.102
A6		2.030	116.1	6.96±0.12[d]	2.22±0.03	1.45±0.04	102.9±3.2	12.897±0.103
A7		2.022	183.9	7.75±0.15[e]	3.16±0.04	2.15±0.02	170.1±3.6	14.139±0.114
B1	[111]	2.027	23.9	5.41±0.10	0.602±0.007	0.388±0.023	22.6±1.3	10.973±0.051
B2		2.029	24.0	5.44±0.11	0.605±0.007	0.389±0.023	22.8±1.3	10.971±0.051
B3		2.009	67.4	6.18±0.12[c]	1.40±0.02	0.915±0.033	58.2±2.3	11.983±0.082
B4		2.043	93.7	6.63±0.07	1.81±0.02	1.18±0.03	79.9±1.9	12.425±0.063
B5		2.027	114.6	6.89±0.12[d]	2.12±0.03	1.38±0.04	97.2±3.0	12.772±0.098
B6		2.034	197.5	7.84±0.16[e]	3.16±0.04	2.13±0.02	171.1±3.7	14.043±0.111
C1	[110]	2.021	23.5	5.51±0.11	0.592±0.006	0.383±0.020	22.2±1.2	10.965±0.045
C2		2.018	67.0	6.17±0.12[c]	1.41±0.02	0.915±0.029	57.9±2.1	11.995±0.075
C3		2.032	90.9	6.59±0.07	1.78±0.02	1.16±0.03	78.1±1.7	12.400±0.058
C4		2.029	112.9	6.91±0.12[d]	2.12±0.03	1.42±0.02	100.6±1.9	12.871±0.063
C5		2.040	193.1	7.88±0.16[e]	3.16±0.04	2.13±0.02	171.8±3.7	14.014±0.111

[a]Eulerian velocity.
[b]These experiments are excluded from further discussions due to inconsistencies mentioned above.
[c]Impactor bowing correction of 4.1±2 ns is applied.
[d]Impactor bowing correction of 2.0±2 ns is applied.
[e]Impactor bowing correction of 29±2 ns is applied.

C. [110] orientation

Figure 4 shows that in experiments C1–C3, a two wave structure was observed. However, a single wave structure was observed in C4 and C5. This observation of an overdriven or a single shock at a lower stress differs from the experiments along the other orientations. However, the particle velocity behind the plastic shock wave and the plastic shock velocity followed the same trend as for other orientations; they increased with increasing impact stress.

D. Comparison between three orientations

The plastic shock velocity and the measured particle velocity behind the plastic shock wave for the three orientations are shown in Table III. We note that in determining the plastic shock wave velocity—when a two-wave structure was measured—the perturbation due to the reflection of the small elastic wave from the Mo–LiF interface was ignored. One can see that, for each elastic impact stress, the plastic shock velocities and the measured particle velocities along the three orientations were in good agreement within experimental uncertainties. For the 23 GPa impact stress experiments (A1, B1, B2, and C1), if one compares experiments A1 and C1, the measured values at the peak state differ by the maxima of experimental uncertainties. For the 66–190 GPa elastic impact stress experiments, measured values at the peak state along the three orientations agree well within the experimental uncertainties, except for the measured particle velocity for experiment A6. This might be attributed to the scatter between samples, but we cannot conclusively account for this difference.

IV. ANALYSIS AND DISCUSSION

A. Determination of in-material quantities

The particle velocity, longitudinal stress, and density at the peak state in Mo single crystals were calculated using the shock jump conditions and the continuity of stress and particle velocity across the surfaces in contact. For the experiments in which the two-wave structure was observed, the wave profile was approximated with two discontinuous steps as shown in Fig. 5. In calculating the peak state for a two-wave structure, the reflection of the elastic wave from the Mo–LiF interface was ignored.

Due to the impedance difference between Mo and LiF, the interaction of the plastic shock wave with Mo–LiF results in a release wave propagating back into Mo. Because the unloading response of Mo single crystals is not accurately known, the following approximation was used to calculate the peak state in the stress–particle velocity plane. The unloading slope was assumed to be bounded by $\rho_0 U^{pl}$ and $\rho_0 U^{el}$, where ρ_0 is the ambient density, and U^{pl} and U^{el} are the Lagrangian plastic and elastic shock velocities, respectively. The peak stress and particle velocity in Mo were calculated using these two slopes, and the calculated values were

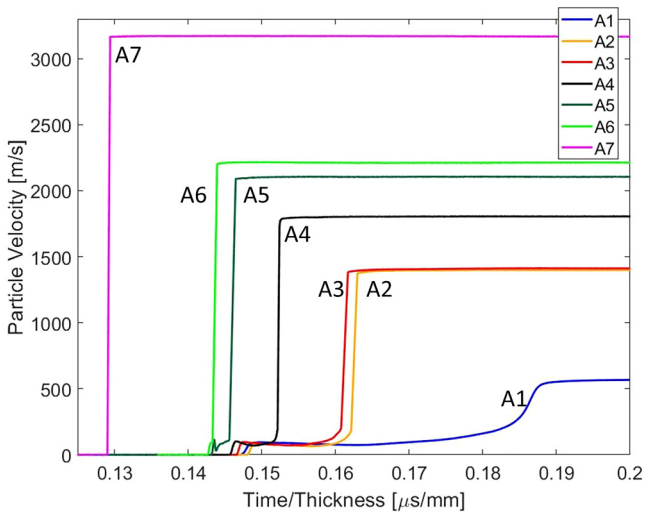

FIG. 2. Measured particle velocity profiles along the [100] orientation.

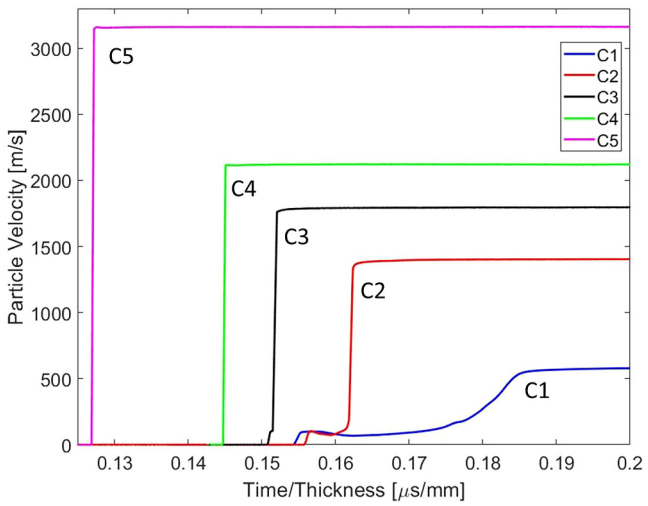

FIG. 4. Measured particle velocity profiles along the [110] orientation.

treated as lower and upper bounds. The known Hugoniot relation for the buffer[25] and the LiF window[26] were used in the calculations. The in-material quantities at the elastic limit[16] were also used.

For the experiments in which the single wave structure was observed, the peak state was calculated using impedance matching with Cu. This is because the unloading response of Mo single crystals from the peak state to the state at the sample/window interface is not accurately known. Although the error bar is larger with calculation using measured particle velocity, two sets of calculation methods give comparable peak states within 1

Table III summarizes the calculated in-material quantities at the peak state along with the plastic shock velocity and the measured particle velocity behind the plastic shock wave. The plastic shock velocity shown in the table is the Eulerian (spatial) velocity U_{Eu}^{pl}. When the two wave structure is observed, that is given by

$$U_{Eu}^{pl} = \frac{\rho_0}{\rho^{el}} U^{pl} + u^{el}, \tag{1}$$

where ρ^{el} is the density at the elastic limit and u^{el} is the in-material particle velocity at the elastic limit.

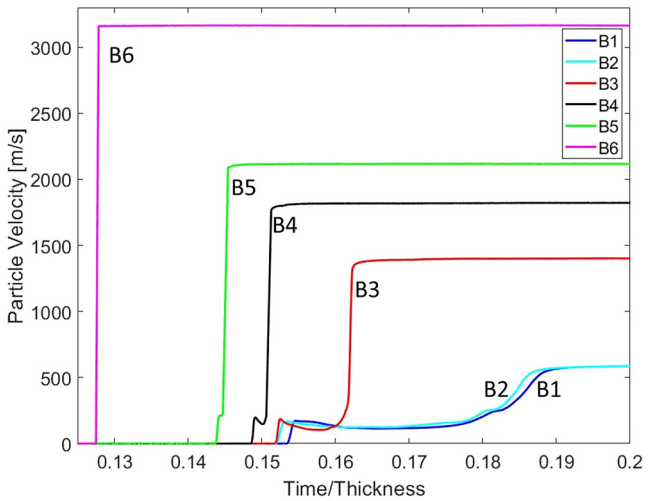

FIG. 3. Measured particle velocity profiles along the [111] orientation.

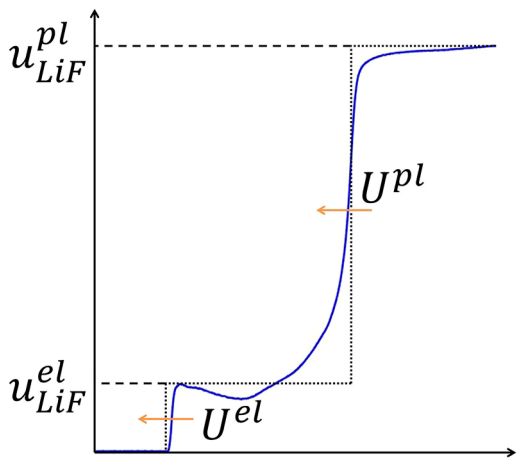

FIG. 5. Two-step approximation of the velocity profiles.

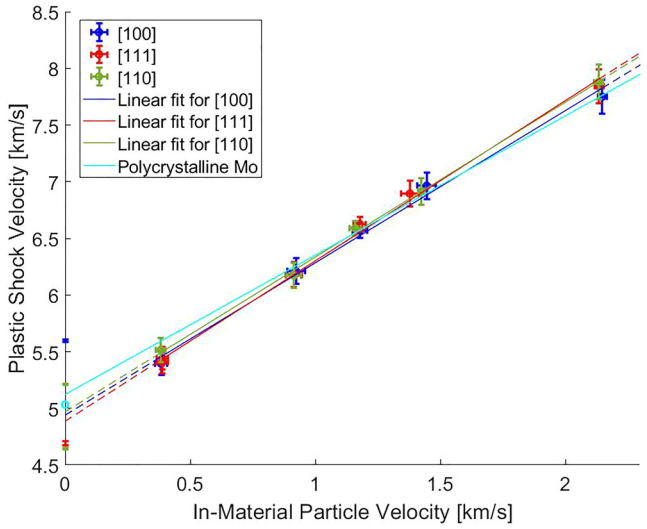

FIG. 6. Shock velocity–particle velocity ($U_s - u_p$) plot at the peak state.

Some noteworthy aspects about Table III are as follows: the expected differences between the elastic impact stresses and the peak stresses; unlike elastic impact stresses, the differences between the in-material quantities at the peak states were within experimental uncertainties.

B. Hugoniot curves for the three orientations

The Hugoniots corresponding to the peak states for Mo single crystals shocked along [100], [111], and [110] orientations, based on results in Table III, are compared next. The plastic shock velocity (U_s) vs in-material particle velocity (u_p) results are shown in Fig. 6. The corresponding longitudinal stress vs volume compression results are shown in Fig. 7. In each figure, Hugoniots for polycrystalline Mo[17] are also shown. A discussion of Figs. 6 and 7 is as follows.

In Fig. 6, the ambient wave velocities shown are the bulk sound speeds corresponding to each Mo single crystal orientation and polycrystalline Mo. For the [110] orientation, two bulk sounds speeds are shown. These correspond to two shear sound speeds as in Table I. Each set of results is fitted with a linear equation using a least squares fit.

The $U_s - u_p$ fits for [100] and [110] orientations are very comparable. Hence, we use a common fit for these two orientations as shown below in Eq. (2).

The fit for the [111] orientation was different from the fit for other two orientations. This is in contrast to Cu[18] and Al[19] single crystals for which indistinguishable response was observed along the three orientations. The plastic shock velocity along the [111] orientation is the lowest in the low stress range ($u_p < 0.6$ km/s) and is the highest in the high stress range ($u_p > 1.9$ km/s). The equations for the linear fits are provided below.

[100]and [110] orientations:

$$U^{pl} = 4.955 + 1.354u_p(\text{km/s}). \quad (2)$$

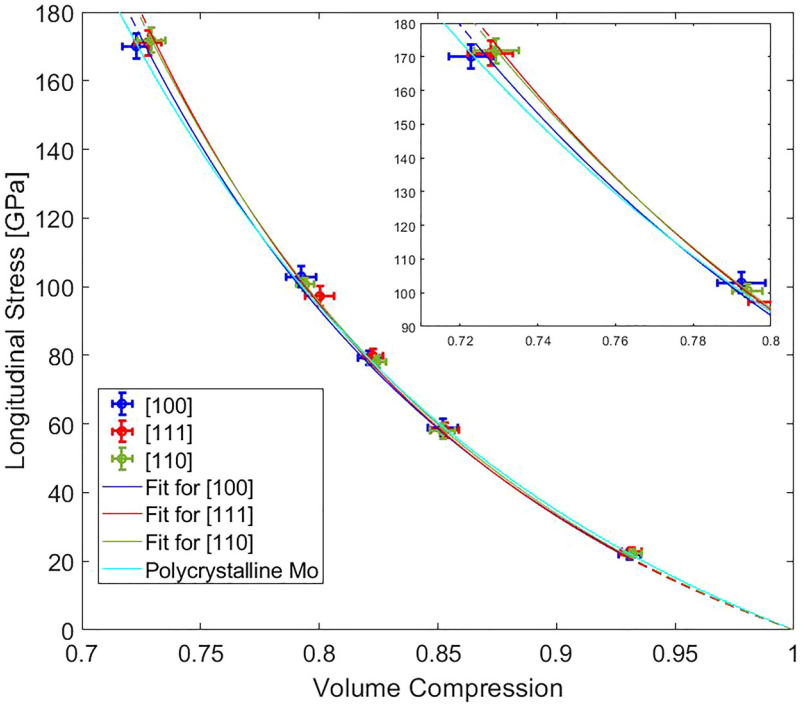

FIG. 7. Longitudinal stress–volume compression ($\sigma_x - v/v_0$) plot at the peak state.

[111] orientation:

$$U^{pl} = 4.886 + 1.415u_p(\mathrm{km/s}). \quad (3)$$

The difference in the constant term in the above equations is within 1.5%. The difference is smaller compared to the difference in the bulk sound speeds for three orientations. However, the difference in the first-order term in Eqs. (2) and (3) is around 5% and shows that the plastic shock velocity along the [111] orientation has stronger dependence on the particle velocity compared to other orientations. Despite these differences in the $U_s - u_p$ response, we note that the differences in the measured plastic shock wave velocities are within experimental uncertainties, as seen in Table III.

The longitudinal stress–volume compression Hugoniots corresponding to the linear fits in Fig. 6 are shown in Fig. 7. As expected, the longitudinal stress along the [111] orientation is the lowest in the low stress range and is the highest in the high stress range. Although the differences shown in Fig. 7 are within experimental uncertainties, they appear to be growing at high stresses—a consequence of differences seen in Fig. 6.

C. Comparison with polycrystalline Mo Hugoniot

In Figs. 6 and 7, the Hugoniot for polycrystalline Mo[17] is shown as the light blue line. While Hixson *et al.*[27] provided Hugoniot data for polycrystalline Mo up to 480GPa, we are using the results from Marsh *et al.*[17] to make comparisons for the stress range examined in the present work. Using a least squares fit, we obtained the following linear equation for the polycrystalline Mo results:

$$U^{pl} = 5.122 + 1.229u_p(\mathrm{km/s}). \quad (4)$$

Both Figs. 6 and 7 show clear differences between Mo single crystals and polycrystalline Mo; however, the differences are within cumulative experimental uncertainties. We note that the polycrystalline Mo displays the smallest slope in Fig. 6. Among the three orientations of Mo single crystals, the Hugoniot for the [100] orientation is the closest to the polycrystalline Mo Hugoniot at high stresses.

D. Discussion

The results related to the peak state measurements were motivated by three broad questions outlined in Sec. I. Below, we address issues raised in each of these questions. To aid the discussion below, we summarize two key findings from our earlier work[16] that was focused on elastic wave amplitudes of shocked Mo single crystals. First, we note that along [100] and [111] orientations, a two-wave structure was observed up to 110 GPa; in contrast, along the [110] orientation, a two-wave structure was observed only to 90 GPa. Second, the elastic wave amplitude increased markedly with elastic impact stress along [111] but the increases along [100] and [110] orientations were quite modest.

Regarding the peak states, the shock response for the [100] and [110] orientations is reasonably similar and suggests that the difference in the overdriving impact stress (110 vs 90 GPa) does not appear to play a significant role. Also, when a two-wave structure is observed, the elastic wave amplitudes are 4–9 GPa. The difference between the three orientation is within the cumulative experimental uncertainties associated with peak stresses. Hence, it is difficult to draw any definitive conclusions.

Although the peak states in shock-compressed Mo single crystals do not show large difference, the response observed for Mo—a BCC crystal—is different from the nearly indistinguishable response observed for Cu[18] and Al[19] single crystals. Thus, the high stress response of BCC and FCC single crystals display differences.

Based on the results obtained in this work, it appears that some anisotropy is manifested in the shock response of Mo single crystals at high stresses (50–190 GPa). In particular, the response along [111] does differ from the response along [100] and [110] orientations and from the response for polycrystalline Mo. Thus, using an isotropic description for high stress peak states in shock-compressed Mo single crystals is likely not valid.

Regarding the shock compression response of Mo single crystals along [111]—manifested by the slope in Fig. 6 which is different from the other two orientations—we note that the elastic amplitude along this orientation showed the largest increase with increasing impact stress. We believe that these two observations for the [111] orientation likely have the same origin —an increase in stress deviators with increasing peak stress. Whether the increase in stress deviators is due to strain hardening and/or mean stress dependence of strength cannot be resolved from our results.

V. SUMMARY

To investigate the peak states achieved in BCC single crystals shocked to high impact stresses, Mo single crystals were subjected to shock compression along [100], [111], and [110] orientations to various impact stresses up to 190 GPa. The present work focused on the peak state, the corresponding Hugoniots, and the comparison of Hugoniots between the three orientations and with polycrystalline Mo. The main findings from the present work are as follows:

- The Hugoniots for the [100] and [110] orientations are comparable to each other. However, the Hugoniot for the [111] orientation is different from the other two orientations. This observation is in contrast to the nearly indistinguishable response observed for Cu and Al single crystals.
- The similarity between the Hugoniots along [100] and [110] orientations suggests that the overdriving impact stress (110 GPa vs 90 GPa) does not play a significant role.
- Despite the difference in the Hugoniots, differences in the in-material quantities at the peak state between three orientations are within cumulative experimental uncertainties.
- Compared to polycrystalline Mo Hugoniot, the Hugoniot for Mo single crystals show clear difference. Among the three orientations, the [100] orientation shows the closest behavior to polycrystalline Mo.
- The difference in the Hugoniot for the three orientations implies that some anisotropy manifests in the shock response of Mo single crystals even at stresses above 100 GPa.

In closing, we note that the present results on Mo single crystals provide a good benchmark for theoretical/computational studies related to understanding condensed matter at high stresses.

ACKNOWLEDGMENTS

We would like to thank Nate Arganbright, Kurt Zimmerman, and Yoshi Toyoda for their help with designing and conducting experiments. We would also like to thank Dr. Michael Winey for his help obtaining known Hugoniot relations and for useful discussions. This work was supported by DOE/NNSA Award No. DE-NA0002007, which is gratefully acknowledged.

DATA AVAILABILITY

The data that support the findings of this study are available within this article and Ref. 16.

REFERENCES

[1]O. E. Jones and J. D. Mote, "Shock-induced dynamic yielding in copper single crystals," J. Appl. Phys. **40**, 4920 (1969).
[2]W. J. Murri and G. D. Anderson, "Hugoniot elastic limit of single-crystal sodium chloride," J. Appl. Phys. **41**, 3521 (1970).
[3]J. R. Asay, G. R. Fowles, G. E. Duvall, M. H. Miles, and R. F. Tinder, "Effects of point defects on elastic precursor decay in LiF," J. Appl. Phys. **43**, 2132 (1972).
[4]Y. M. Gupta, "Elastic compression to 30 kbar along ⟨111⟩ in shocked LiF," Appl. Phys. Lett. **26**, 38 (1975).
[5]L. E. Pope and J. N. Johnson, "Shock-wave compression of single-crystal beryllium," J. Appl. Phys. **46**, 720 (1975).
[6]Y. M. Gupta, "Effect of crystal orientation on dynamic strength of LiF," J. Appl. Phys. **48**, 5067 (1977).
[7]G. I. Kanel and S. V. Razorenov, "Anomalies in the temperature dependences of the bulk and shear strength of aluminum single crystals in the submicrosecond range," Phys. Solid State **43**, 871 (2001).
[8]H. Huang and J. R. Asay, "Reshock response of shock deformed aluminum," J. Appl. Phys. **100**, 043514 (2006).
[9]G. Whiteman, S. Case, and J. C. F. Millett, "Planar shock compression of single crystal tantalum from 6–23 GPa," in *Journal of Physics: Conference Series* (IOP Publishing, 2014), Vol. 500, p. 112067.
[10]J. M. Winey, P. Renganathan, and Y. M. Gupta, "Shock wave compression and release of hexagonal-close-packed metal single crystals: Inelastic deformation of c-axis magnesium," J. Appl. Phys. **117**, 105903 (2015).
[11]A. Mandal, "Elastic-plastic deformation of molybdenum single crystals shocked to 12.5 GPa," Ph.D. thesis (Washington State University, School of Mechanical and Materials Engineering, 2016).
[12]P. Renganathan, J. M. Winey, and Y. M. Gupta, "Shock compression and release of a-axis magnesium single crystals: Anisotropy and time dependent inelastic response," J. Appl. Phys. **121**, 035901 (2017).
[13]A. Mandal and Y. M. Gupta, "Elastic-plastic deformation of molybdenum single crystals shocked along [100]," J. Appl. Phys. **121**, 045903 (2017).
[14]A. Mandal and Y. M. Gupta, "Elastic-plastic deformation of molybdenum single crystals shocked to 12.5 GPa: Crystal anisotropy effects," J. Appl. Phys. **125**, 055903 (2019).
[15]J. Millett, P. Avraam, G. Whiteman, D. Chapman, and S. Case, "The role of orientation on the shock response of single crystal tantalum," J. Appl. Phys. **128**, 035104 (2020).
[16]T. Oniyama, Y. M. Gupta, and G. Ravichandran, "Shock compression of molybdenum single crystals to 110 GPa: Elastic-plastic deformation and crystal anisotropy," J. Appl. Phys. **127**, 205902 (2020).
[17]S. P. Marsh, *LASL Shock Hugoniot Data*, Vol. 5 (University of California Press, 1980).
[18]R. Chau, J. Stölken, P. Asoka-Kumar, M. Kumar, and N. C. Holmes, "Shock Hugoniot of single crystal copper," J. Appl. Phys. **107**, 023506 (2010).
[19]D. Choudhuri and Y. M. Gupta, "Shock compression of aluminum single crystals to 70 GPa: Role of crystalline anisotropy," J. Appl. Phys. **114**, 153504 (2013).
[20]A. C. Mitchell and W. J. Nellis, "Shock compression of aluminum, copper, and tantalum," J. Appl. Phys. **52**, 3363 (1981).
[21]L. M. Barker and R. E. Hollenbach, "Laser interferometer for measuring high velocities of any reflecting surface," J. Appl. Phys. **43**, 4669 (1972).
[22]L. M. Barker and K. W. Schuler, "Correction to the velocity-per-fringe relationship for the VISAR interferometer," J. Appl. Phys. **45**, 3692 (1974).
[23]D. H. Dolan, "Foundations of VISAR analysis," Sandia National Laboratories Report No. SAND2006–1950, 2006.
[24]D. Choudhuri and Y. M. Gupta, "Shock compression and unloading response of 1050 aluminum to 70 GPA," AIP Conf. Proc. **1426**, 755 (2012).
[25]M. D. Knudson and M. P. Desjarlais, "Adiabatic release measurements in α-quartz between 300 and 1200 GPa: Characterization of α-quartz as a shock standard in the multimegabar regime," Phys. Rev. B **88**, 184107 (2013).
[26]P. A. Rigg, M. D. Knudson, R. J. Scharff, and R. S. Hixson, "Determining the refractive index of shocked [100] lithium fluoride to the limit of transmissibility," J. Appl. Phys. **116**, 033515 (2014).
[27]R. S. Hixson and J. N. Fritz, "Shock compression of tungsten and molybdenum," J. Appl. Phys. **71**, 1721 (1992).